Received: 19 March 2024 | Revised: 30 April 2024 | Accepted: 7 June 2024

DOI: 10.1111/jace.19967

Journal of the American Ceramic Society

RESEARCH ARTICLE

SiOC foam-aerogel composites: Optimal balance of lightness and excellent thermal insulation

Oyku Icin[1] | **Adane Muche Abebe**[2] | **Gian Domenico Soraru**[2] | **Cekdar Vakifahmetoglu**[1]

[1]Department of Materials Science and Engineering, İzmir Institute of Technology, Izmir, Turkey

[2]Department of Industrial Engineering, University of Trento, Trento, Italy

Correspondence
Cekdar Vakif Ahmetoglu, Department of Materials Science and Engineering, İzmir Institute of Technology, Izmir 35433, Turkey.
Email: cekdarvakifahmetoglu@iyte.edu.tr, cvahmetoglu@gmail.com

Funding information
TUBITAK (The Scientific and Technological Research Council of Turkey), Grant/Award Number: 122M533; AFOSR, Grant/Award Number: FA9550-21-1-0279

Abstract

Foam-aerogel composites are synthesized in polymeric, hybrid, and ceramic states by completing the open cells of the foam with a solution forming a wet gel, carbon dioxide (CO_2) supercritically dried, and pyrolyzed. Thermal diffusivity measurements are conducted using the laser flash, and for mechanical performance, cold crushing tests are done to obtain compressive strengths. Samples possess a range of specific surface area (SSA) values up to ~650 m^2/g contingent upon the material state, that is, polymeric, hybrid, or ceramic. While SSA values can be deliberately altered, almost all samples demonstrated a total porosity of ~90 vol%, with superb specific compressive strength reaching around 2 MPa. In addition to adjustable surface characteristics granting hydrophobic and hydrophilic features, the study revealed the potential use of these foam-aerogel composites as thermal insulators with low thermal conductivities of 0.02 $W{\cdot}m^{-1}{\cdot}K^{-1}$ at RT and 0.05 $W{\cdot}m^{-1}{\cdot}K^{-1}$ at 500°C. When exposed directly to a butane flame gun with a flame temperature reaching ~1200°C, from the backside of a 5 mm-thick foam-aerogel composite, only ~200°C is recorded, which is lower than a comparable commercial insulator panel tested under the same conditions.

KEYWORDS
aerogels, composite, foam, SiOC, thermal insulation

1 | INTRODUCTION

Porous ceramics are employed in diverse engineering applications ranging from water purification, insulation, and filtration to building blocks.[1] Porous polymer-derived ceramics (PDC) is a class of advanced ceramics formed using preceramic polymers or via the sol-gel route following several different processing techniques.[2,3] Conventionally, foams have randomly distributed pores (open-cells have three-dimensional [3D]-interconnected pores allowing fluid permeability), defined with pores per inch (PPI) and relative density generally below 0.3, that is, total porosity > 70 vol%.[4] The replica method is one of the most straightforward approaches for foam processing, particularly in producing PDC foams, due to the simplicity of controlling the processing conditions.[5]

Compared to foams, aerogels are a peculiar class of porous components with a much smaller scale of pores,

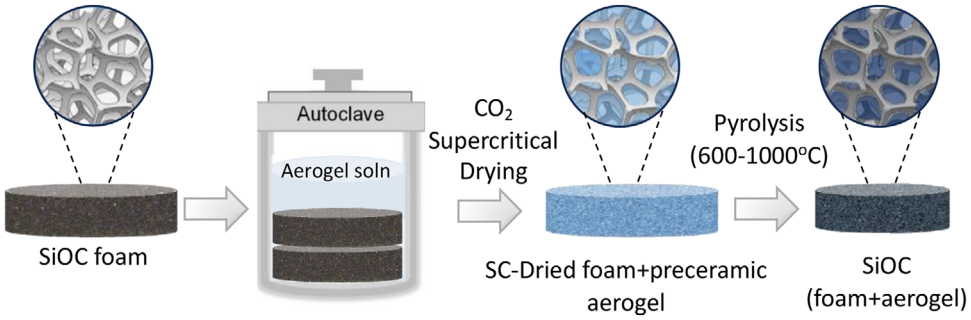

FIGURE 1 Preparation process of SiOC foam-aerogel composite.

that is, roughly speaking below 100 nm, and with very high porosity, making them one of the lowest relative density solids. A considerable effort has been devoted to forming aerogels with different compositions and exploring their applications, including thermal insulation,[6] energy storage,[7] acoustic insulation,[8] catalyst supports,[9] environmental remediation,[10] and aerospace[11] due to their high porosity (usually > 80 vol%) and specific surface area (~100–1000 m^2/g).[12]

PDC aerogels have gained increasing attention in recent years due to intriguing properties compared to silica aerogels and many other lightweight materials.[13] Their high thermal stability and electrical characteristics make them promising candidates for different applications.[2] However, regardless of the aerogel chemistry, there are well-known problems and limitations to processing monolithic parts, complex shapes, and decent mechanical integrity.

Accordingly, to alleviate the problems mentioned, a few strategies have already been employed, such as incorporating fibers or particles into the aerogel structure.[14–18] Others proposed the formation of strength-improved composite structures achieved by using porous substrates (e.g., PU, carbon, SiC, and glass).[19,20,21–32] In this context, for the first time here, the SiOC foam/aerogel composites were designed to demonstrate the manufacturing feasibility of highly porous aerogel monoliths, which can be machinable into a variety of forms while preserving their insulating abilities and mechanical properties.

2 | EXPERIMENTAL PROCEDURE

2.1 | Materials

A commercial poly(methylsilsesquioxane) (PMS) preceramic polymer was obtained from Wacker GmbH (MK Belsil, Wacker GmbH). Tin(II) 2-ethylhexanoate was purchased from Sigma- Aldrich (Tin, CAS: 301-10-0, USA) and diluted 15% vol. in xylene (ACS reagent ≥99.8%, Merck, CAS:1330-20-7). Acetone (extra pure grade, Tekkim, CAS: 67-64-1) was used as the solvent. 90 PPI PU foams with an open cell structure (A.R.E.) were used as a template for preparing PDC foams. CO_2 (99.5%) was used for the supercritical drying (SC-Drying) process.

2.2 | Foams

PMS resin-derived SiOC foams were prepared via replica technique using flexible PU foams (90 PPI) as template/substrate. The preceramic resin and PU foam recipe were prepared as PU/PMS/Acetone = 1:2:20 in weight ratio. Initially, PU foams were cut into desired sizes (diameter of ~35 mm and thickness of ~5 mm), and solid PMS resin powder was dissolved in acetone while stirring at 500 rpm at room temperature (RT) for 10 min. The resulting solutions were then transferred into separate glass Petri dishes, and foams were impregnated with a solution following a previously published procedure.[5,33] After the drying step of 1 h, the curing procedure was carried out at 200°C for 6 h. Finally, all the cured foams were pyrolyzed under Argon (Ar) flow (200 mL/min) at two different temperatures (400 and 1000°C) in an alumina tube furnace PROTERM PTF 16/75/450, Ankara, Turkey) with a heating rate of $2°C.min^{-1}$ for 2 h (dwell time). Pyrolyzed foams were coded as follows: P4 (at 400°C), and P10 (at 1000°C) according to pyrolysis temperature.

2.3 | SiOC foam/aerogel composites

The foam-preceramic aerogel composites were produced by four basic steps, as depicted in Figure 1. First, the sol of the preceramic polymer (PMS) was prepared accordingly: PMS was dissolved in acetone (75 vol% of the prepared sol), and the solution was stirred at 500 rpm for 20 min, following the addition of tin catalyst (3.75 vol% of PMS precursor) with the procedure previously described.[34]

The obtained sol was poured into the Teflon liner containing the prepared PU90-PMS derived foams (P4 or

P10) for the composite synthesis until completely covered. Cross-linking of aerogel sol with the pretreated foam was conducted in an autoclave (55% filling, at 200°C for 6 h in a stainless-steel autoclave, 4748 model; Parr) to prevent solvent evaporation. The autoclave was then cooled to RT, and the foam-preceramic gel composites were de-molded and washed with fresh acetone (twice/day for 3 days). Foam-preceramic gels were dried by SC-Drying using CO_2 at 50°C, with a pressure of 150 bar. Finally, all the dried foam-preceramic aerogel composites were pyrolyzed at different temperatures (at 600 and 1000°C, with a heating rate of 2°C/min) in an alumina tube furnace (PROTERM PTF 16/75/450) in a flowing Ar atmosphere (a flow rate of 200 mL/min), and with a 2 h dwell time.

2.4 | Characterization

The morphologies of preceramic and pyrolyzed foam-aerogel composites were analyzed using scanning electron microscopy (SEM; FEI Quanta 250 FEG). The fractured surface of composites was coated with ~10 nm Au layer by sputtering (Emitech K550X sputter coater; Quorum Technologies) before the SEM analysis. SEM images were subsequently analyzed using the ImageJ software (ImageJ 1.52a; National Institutes of Health) to quantify the strut or cell size and distribution. The average data (from 50 measurements) obtained by image analysis were converted to 3D values by applying the stereological equation: $D_{sphere} = D_{circle}/0.785$ to get the effective cell dimension.[33]

Fourier transform infrared spectra (Spectrum Two FT-IR with UATR fitted; PerkinElmer) were recorded in the range of 450−4000 cm^{-1} with 20 scans and 4 cm^{-1} resolution in the transmission mode to investigate structural features of composites. X-ray diffraction (XRD; Bruker D8 Advance) data were collected using the Cu K_α radiation (between 2θ; 20–90°, step counting time of 0.1 s, and scan of 0.2°). The FTIR and XRD data were plotted after normalization. Raman spectra were recorded with Renishaw InVia Qontor Raman spectrometer, using a laser (532 nm), and 10% power on the sample with a 10-s exposure in the wavenumber region 1000−2000 cm^{-1}, using 50× objective lens giving a laser spot diameter of 5 μm.

Nitrogen (N_2) sorption analyses were performed using a Micrometrics 3FLEX-Adsorption Analyzer. The samples were degassed at 200°C for 24 h before the examination. SSA was determined from a Brunauer–Emmett–Teller (BET) approach. The Barrett-Joyner-Halenda was used to obtain the pore size distribution. Wetting behavior was analyzed using the theta model contact angle (CA) measurement device (KSV-Attension brand). The contact angle measurement was carried out from the digital photos of 5 μL of distilled water deposited on the top surface of the samples.

The bulk density was determined at room temperature using Archimedes' displacement technique with ethanol as the buoyancy fluid. The true densities of the samples were acquired using an Anton Paar Ultrapyc 5000 Helium Pycnometer, and the total porosities were subsequently calculated.

Thermal diffusivity (α) of samples was measured with the laser flash diffusivity method using a Netzsch 467 HyperFlash (Selb, Germany) on square specimens (side length = 10 mm). Measurements were carried out by applying a self-regulating pulse width of 0.6 ms, a laser voltage of 250 V, and a spot amplitude of 3.7 mm within the temperature range from 25 to 500°C (instrument limit). The penetration model was used to fit the output curve. The total thermal conductivity values (k) were calculated using the formula $k = \alpha \times C_p \times \rho$, where ρ is the bulk density of aerogel and Cp is the specific heat capacity. The specific heat capacity values (C_p) were extracted from the published data on a similar SiOC system (0.75–1.12 $J.g^{-1}.K^{-1}$ between 25 and 500°C).[35] To further test the thermal properties, the cylindrical sample (diameter 2.5 cm and thickness 5 mm) was fixed into a cylindrical hole made in the commercial Xonotlite (Promaton) panel (PROMASIL 1000L), having a bulk density of 0.3 g/cm^3, total porosity: ~90 vol%, thermal conductivity: 0.08 (at RT) and 0.16 $W.m^{-1}.K^{-1}$ (at 800°C), and compressive strength: 2.5 MPa) used for thermal insulation. The sample was hit with a butane flame gun, and the backside temperature was recorded by a thermal infrared imager (FLIR ThermaCAM PM695).

The compression tests of neat foams, aerogels, and their composites were carried out by using an Instron 5969, equipped with an Instron 2518−804 load cell (10 kN), and applying a compression speed of 0.8 mm/min. The average compression test data were acquired from at least five samples with a ~5 × 5 × 5 mm^3 cubic shape.

3 | RESULTS AND DISCUSSION

3.1 | Microstructural

Figure S1A–G displays the digital photos of foam-aerogel composites. Bluish samples were obtained by impregnating the gels into foam cells and CO_2 SC-Drying. When substrate foams to be used for impregnation were initially pyrolyzed at 400°C they were marked as P4 (see Figure S1A), and the ones obtained via 1000°C pyrolysis as P10 (see Figure S1D).

Upon pyrolysis of the foam-aerogel composite at 600°C, regardless of which temperature the parent substrate

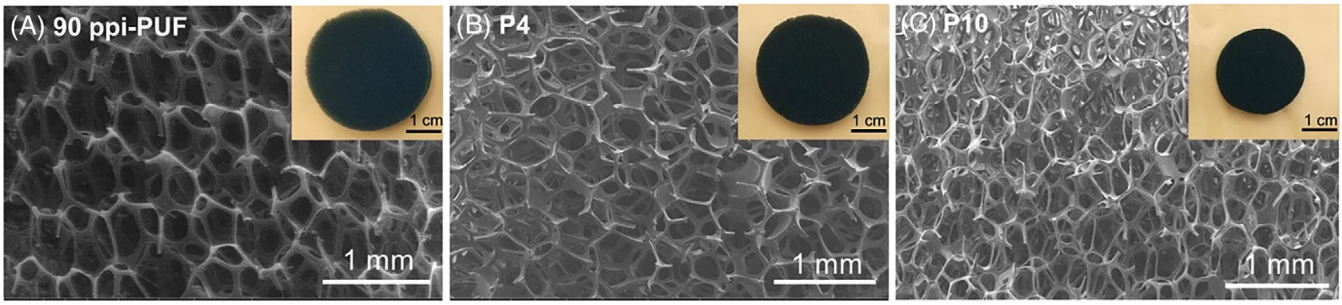

FIGURE 2 Scanning electron microscopy (SEM) and digital images of the foams (A) as received PU (90 PPI), (B) impregnated with preceramic blend and pyrolyzed at 400°C (P4), and (C) when pyrolysis was conducted at 1000°C (P10).

foams were made, both samples turned to dark gray, see Figure S1b,e, then totally black when the pyrolysis temperature was increased to 1000°C, Figure S1C,F. In addition to cylindrical samples, hollow monoliths and machined complex shapes (e.g., a star, see Figure S1G) were also produced to illustrate the potential of the new processing approach.

The linear shrinkage values were calculated for the samples pyrolyzed at 1000°C; reached around 25% for 400°C pyrolyzed-foam-based composite (P4-A-1000), whereas there was no shrinkage for the 1000°C pyrolyzed-foam-based composite ones (P10-A-1000), predictably.

SEM micrographs and digital images for the received 90PPI-PU foam (PU90, cell size: 616.9 ± 68.7 μm, strut thickness: 52.6 ± 9.1 μm) and PU90-PMS derived foams are given in Figure 2. PDC replica foams (P4 and P10) have open-cell 3D networks similar to parent PU foam. Cell sizes and strut thickness of the PDC foams were measured as 652.1 ± 110.2 μm and 36.1 ± 9.2 μm, resulting in no linear shrinkage when pyrolysis was conducted at 400°C (P4). Increasing the pyrolysis temperature to 1000°C (P10) leads to a cell size and strut thickness of 517.3 ± 83.2 μm and 23.7 ± 5.5 μm, with a linear shrinkage of 20%. Besides, both foams have ~96 vol% total porosity.

Figure 3A,B shows the fracture surface microstructures of aerogel composites made by impregnating the 400°C -pyrolyzed foam (P4-composite series) with preceramic aerogel after SC-Drying. As can be seen, remarkably, the solidified aerogel entirely filled the cells. When such a composite system was pyrolyzed at 600°C, cohesion between the parent foam (P4) struts and SC-dried preceramic aerogel fillings remained intact, Figue 3C,D. It can be argued that such a full coverage of the foam cells was obtained for the first time, which can be explained by the similar shrinkage of the foam and aerogel structures up to such pyrolysis temperature. When the pyrolysis temperature was raised to 1000°C, scarce interfacial gaps were observed between foam struts and aerogels due to limited shrinkage differences, see Figure 3E,F. This is similar to previous data,[34] in which neat SC-Dried aerogel showed ~24% linear shrinkage at 1000°C pyrolysis, while shrinkage of the preceramic foam reached 20% (note here that the parent foam, P4, was already treated at 400°C).

The SEM micrographs of the 1000°C-pyrolyzed foam (P10-composite series)-based aerogel composites are presented in Figure S2. When P10 foam was used to be infiltrated, dissimilar shrinkage behavior of the aerogel precursor and the substrate foam resulted in the formation of large cavities. Specifically, during the pyrolysis of P10-foam-based aerogel composites, shrinkage was almost negligible for pre-pyrolyzed (1000°C) P10 foam compared to aerogel precursor, which shrunk more significantly than the foam matrix, see Figure S2C.

3.2 | Structural

Thermogravimetric analysis (TGA) data of the PU foam, parent foam (pyrolyzed at 400 and 1000°C), and SC-dried foam-aerogel composites are given in Figure 4A and Figure S3A. According to TGA results of neat PU foam, the most prominent weight loss occurred between 250 and ~450°C, showing 98.3% weight loss at 1000°C. When the pre-pyrolyzed P4 foam is examined, it is clear that there is no weight loss up to 470°C, indicating the received PU foam is completely decomposed. Starting at 630°C and ending at ~800°C, the weight loss is due to mineralization of PMS polymer. In the case of the foam-aerogel composite, P4-A-Polymer has a weight loss of around 15%. The most significant contribution was polymeric aerogel ceramization between 480 and 800°C. The ceramic yield was ~85% at peak test temperature (1000°C).

For TGA data of parent P10 foam and P10-foam-based composite (see Figure S3A), no weight loss was observed for parent foam (P10) during the second heat treatment at 1000°C under N_2 atmosphere. The weight loss in the foam-aerogel composite (P10-A-Polymer) was only due to the conversion of SC-Dried polymeric aerogel to ceramic. This explains the gaps between the foam and aerogel, discussed above, based on SEM images (see Figure S2).

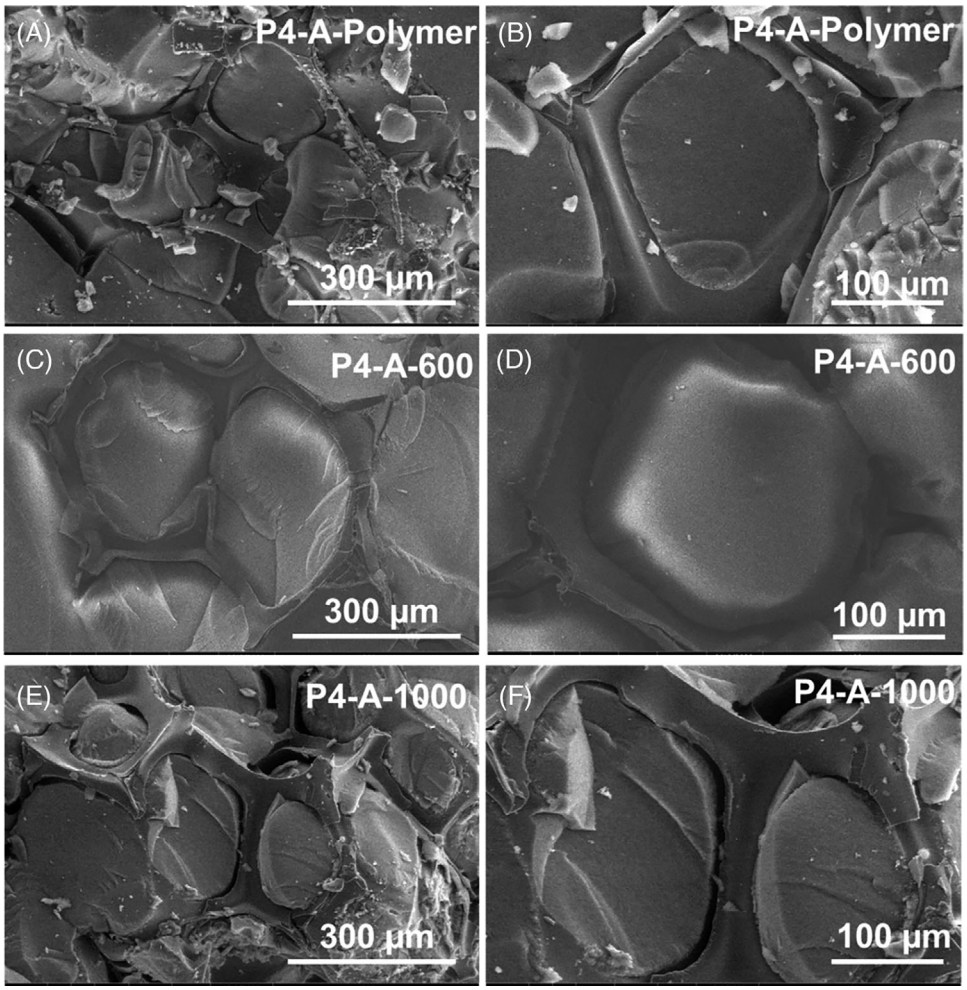

FIGURE 3 Scanning electron microscopy (SEM) images of preceramic polymer derived foam-aerogel composites produced using foam pyrolyzed at 400°C (P4); (A, B) Supercritical dried (SC-Dried) aerogel impregnated P4 foam (P4-A-Polymer), (C, D) The same impregnated system when pyrolyzed at 600°C (P4-A-600), and (E, F) The same impregnated system when pyrolyzed at 1000°C (P4-A-1000).

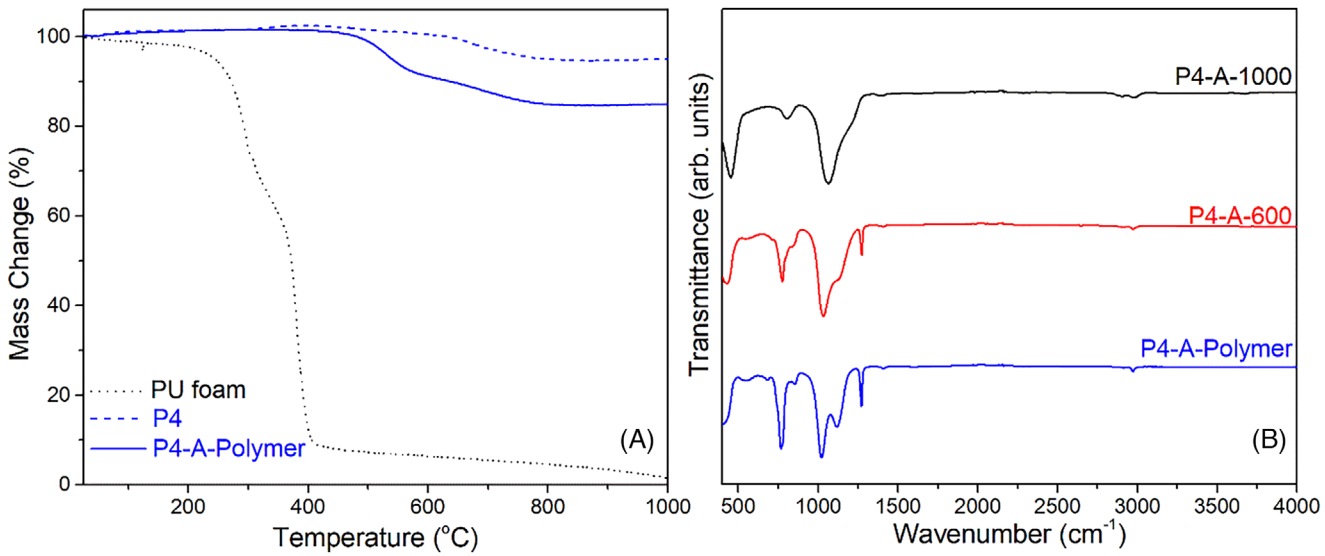

FIGURE 4 (A) Thermogravimetric analysis (TGA) data (5°C /min; N_2 flow) of PU foam, parent foam pyrolyzed at 400°C (P4), and supercritical dried (SC-Dried) aerogel impregnated P4 foam (P4-A-Polymer) and (B) Fourier-transform infrared (FTIR) spectra foam-aerogel composites produced using foam already pyrolyzed at 400°C (P4).

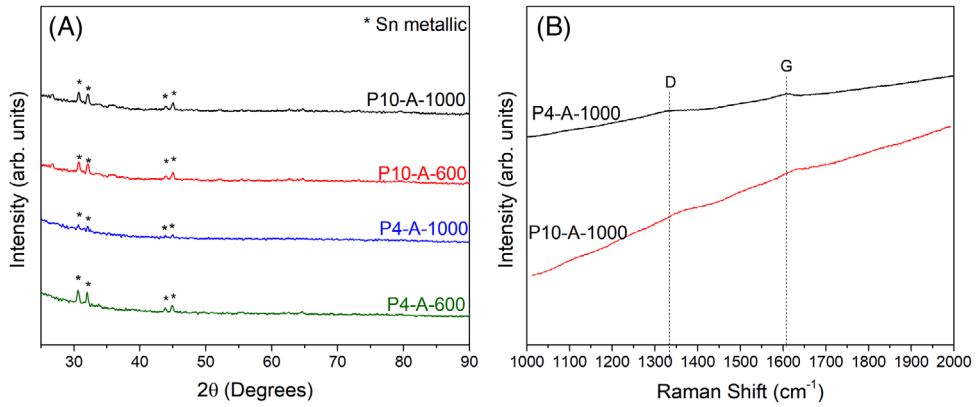

FIGURE 5 (A) Normalized X-ray diffraction (XRD) patterns (reference reflection marks for metallic Sn (ICDD PDF # 01-086-2264) are given at the top of the experimental data), and (B) Raman spectra of SiOC foam-aerogel composites.

The FTIR spectra of the foam-aerogel composites produced using 400°C pre-pyrolyzed (P4) foam and 1000°C-pyrolyzed (P10) foam are given in Figure 4B and Figure S3B, respectively. The characteristic vibration bands associated with the Si–CH_3 groups in the PMS polymer, specifically at 770 and 1270 cm^{-1}, are still evident in the P4-A-Polymer and P4-A-600 composites. However, these bands disappear following the pyrolysis at 1000°C. In the FTIR spectra given in Figure 4 and Figure S3, SiOC foam-aerogel composites (P4-A-1000 and P10-A-1000) exhibit three prominent signals: (i) the Si—O bond corresponding to Si—O—Si deformation at 451 cm^{-1}, (ii) at ~800 cm^{-1} arising from Si–C and Si–O stretching, and (iii), a broad peak of Si—O stretching due to Si—O—Si vibrations around 1065 cm^{-1} within the silicon oxycarbide network.[33,34]

Figure 5A shows the XRD patterns of pyrolyzed foam-aerogel composites. The data revealed only the presence of metallic tin (ICDD PDF # 01-086-2264) resulting from the catalyst decomposition and reduction during the pyrolysis, similar to previous work.[34] Raman data of SiOC foam-aerogel composites (obtained by 1000°C pyrolysis) are given in Figue 5B. The characteristic two in-plane modes, the D-mode (at 1330 cm^{-1}) and the G-mode (at 1600 cm^{-1}) were overlaid by a pronounced fluorescence background typical of SiOC pyrolyzed at low temperature (ca 1000/1200°C).[36–38]

3.3 | Porosity and surface

Figure 6 illustrates the N_2 sorption isotherms of foam-aerogel composites at 77 K. According to the IUPAC classification, P4-A-Polymer, P4-A-600, and P4-A-1000 (SiOC) display Type IV isotherms with a hysteresis loop resembling the H1 characteristic, indicating cylindrical pores and agglomerates. In a similar fashion, foam-aerogel composites made using a pre-pyrolyzed foam at 1000°C, P10-A-Polymer, P10-A-600, and P10-A-1000, display Type IV isotherms and H1-type hysteresis (Figure 6B).

The calculated BET specific surface area (SSA) values of P4-A-Polymer (644 m^2/g) and P4-A-600 (503 m^2/g) were higher than that of the P10-A-Polymer (507 m^2/g) and P10-A-600 (320 m^2/g). The difference may originate from having a lower temperature pre-pyrolyzed (400°C, P4) foam matrix (with an SSA of 69.5 m^2/g), resulting in transient porosity.[39] After pyrolysis 1000°C, obtained SiOC foam-aerogel composites yielded similar SSA values as 236 m^2/g (P4-A-1000) and 169 m^2/g (P10-A-1000), while the parent foam substrate had only 1.2 m^2/g, indicating the efficacy of the employed composite design.

Contact angles were measured as 140 ± 25° (P4-A-Polymer), 114 ± 20° (P4-A-600), and 24 ± 12° (P4-A-1000), as illustrated in Figure 7. The polymeric foam-aerogel composite was characterized by a strong hydrophobic behavior with apparent contact angles as high as ≈ 140°. A direct association was observed between the contact angle and the elevated pyrolysis temperature, leading to a change from hydrophobic to hydrophilic transformation, akin to previous works.[34,40] A similar trend was observed for P10-foam-based aerogel composite systems (see Figure S4).

3.4 | Mechanical and thermal

The compressive strength-versus total porosity graphs of the foams, aerogels, and foam-aerogel composites are presented in Figure 8. Bulk density, total porosity, and compressive strength value of foams, aerogels, and foam-aerogel composites were also given in Table S1.

PU-derived foams, obtained by pyrolysis at different temperatures (P4; 400°C, P6; 600°C, and P10; 1000°C), gave compressive strength values reaching 0.123 ± 0.057 MPa for P10. The compressive strength of parent foams increased with pyrolysis temperature.

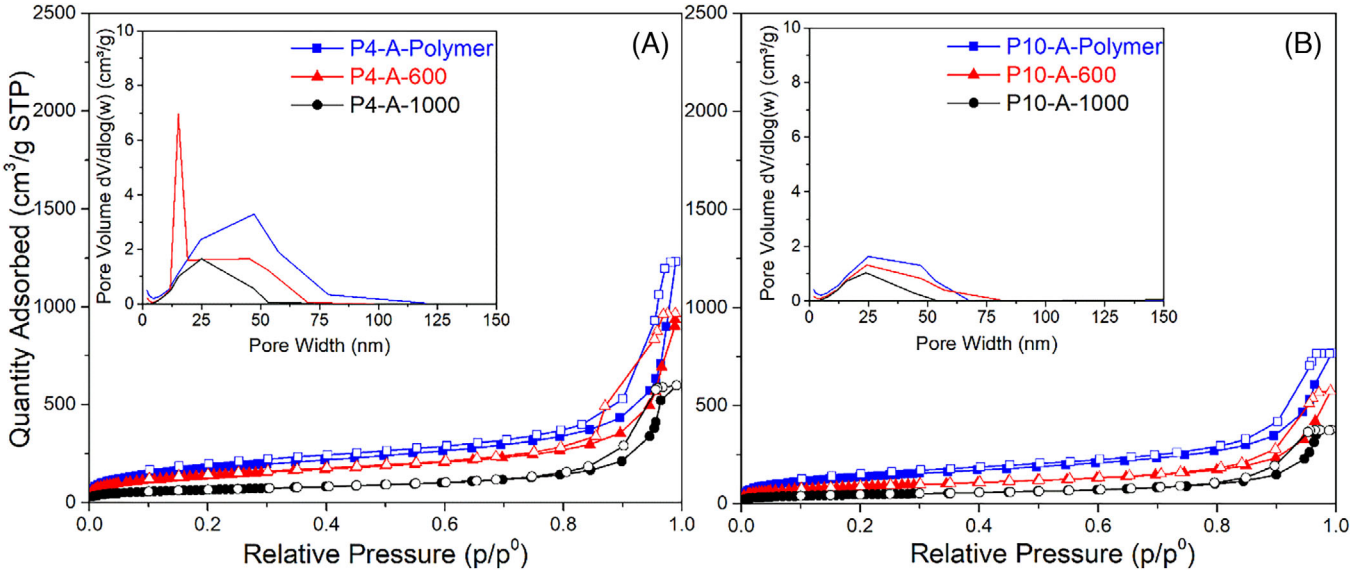

FIGURE 6 N_2 sorption isotherms of foam-aerogel composites produced using foam (A) already pyrolyzed at 400°C (P4) and (B) already pyrolyzed at 1000°C (P10). (the top-left insets represent the pore size distribution curves).

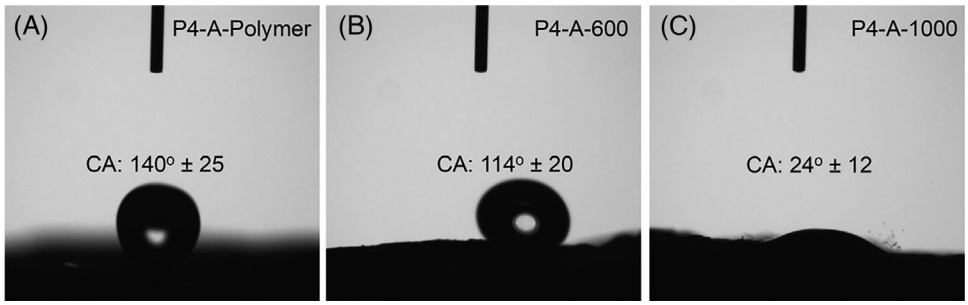

FIGURE 7 Digital images demonstrate wetting behavior from the angles of water droplets on foam-aerogel composite surface produced using foam pyrolyzed at 400°C (P4); (A) Supercritical dried (SC-Dried) aerogel impregnated P4 foam (P4-A-Polymer), (B) The same impregnated system when pyrolyzed at 600°C (P4-A-600), and (C) The same impregnated system when pyrolyzed at 1000°C (P4-A-1000).

Corresponding compressive strength values for SiOC foams, having a high porosity (total porosity of around 96 vol%), were similar to other polymer-derived foams.[32,33,41]

The neat aerogels possessed decent compressive strength ranging from 0.419 ± 0.085 MPa for a polymeric one and 3.239 ± 1.197 MPa for a SiOC ceramic (A-1000) with ~75–80 vol% total porosity, akin to that of SiOC, SiC and silica aerogels reported in the literature.[42–46] Indeed, when thermoset aerogels were pyrolyzed, the bonding strength of the particles forming aerogel enhanced, yielding a more robust material. However, a high standard deviation emphasizes the challenges in sample preparation.

The aerogel-filled foam composites showed intermediate mechanical properties between the mother substrate foams and those of the neat aerogels. Compared to substrate foam with a bulk density of 0.05–0.09 g/cm^3, the higher bulk density (0.21–0.24 g/cm^3) observed in composite structures contributed to the improved mechanical properties. For a monolith (P4-A-1000) with 90 vol% total porosity, high strength approaching around 2 MPa was recorded; see Figure 8. Load-extension graphs of P4 foam-based composites were also given in Figure S5. The graphs illustrate a trend wherein strain reduces while strength increases when transitioning from polymeric composites to ceramics.

The differences in the strength values of foams, aerogels, and foam-aerogel composites can be attributed to the combined effect of pore size and total porosity. A trend was that the higher the total porosity and pore size, the lower the strength was noted. In addition, increased pyrolysis temperature yielded the formation of stronger articles. Although the bulk density and total porosity values of the final SiOC foam-aerogel composites (P4-A-1000 and P10-A-1000) were very similar, P4-A-1000 showed about ten

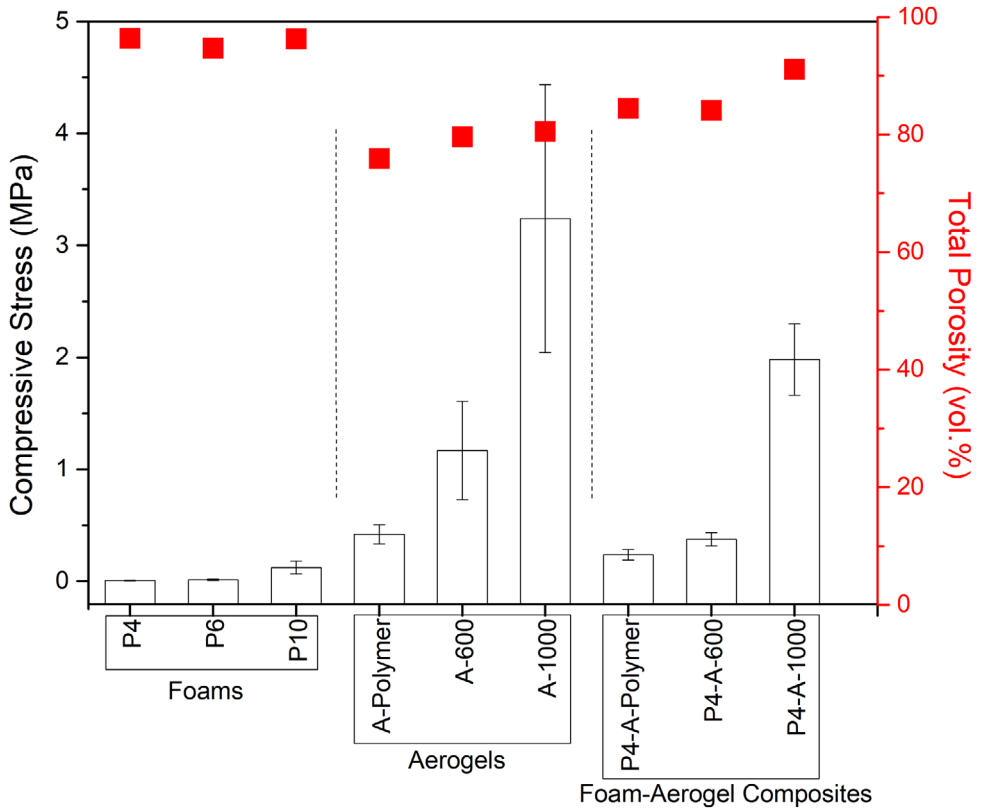

FIGURE 8 Total porosity (vol%) vs. compressive strength (MPa) graph of tested samples; Foams pyrolyzed at 400°C (P4), 600°C (P6), and 1000°C (P10), Aerogels: Supercritical dried (SC-Dried) (A-Polymer), pyrolyzed at 600°C (A-600), and pyrolyzed at 1000°C (A-1000), and Foam-Aerogel Composites produced using foam pyrolyzed at 400°C (P4 foam-based).

times higher compressive strength than P10-A-1000, which might simply be explained by the microstructural differences, that is, the large cavities between struts and aerogel of P10-A-1000 system compared to fully covered, coherent P4-A-1000 system, probably yielding much better load distribution, less stress intensity points, etc., see in Figure S2C and Figure 3E,F.

Here, we only provide details on similar systems. In our recent study,[32] silicon carbide (SiC) foam-aerogels with ~90 vol% total porosity showed a compressive strength below 0.77 MPa. Similar low values were seen in the study of Ye et al.[27] in which reticulated SiC skeleton-reinforced silica aerogel composites were made, and the compressive strength value was found as ~0.03 MPa with a porosity of 30.8 vol%. Liu et al.[31] prepared carbon foam/silica aerogel composite and found that the maximum compressive strength was about 1.0 MPa. In addition, the compressive strength values below 0.5 MPa were documented for carbon foam-reinforced carbon aerogel obtained by 900°C pyrolysis; however, the total porosities were not given in those, but only bulk density was reported as 0.08–0.10 g/cm^3.[20] As seen, while the literature does not provide sufficient data, we can still speculate that the foam-aerogel composite system manufactured here exhibited excellent mechanical properties compared to those given above.

Temperature-dependent thermal diffusivity and conductivity values of the foam-aerogel composites are given in Figure 9. According to the laser flash diffusivity, at RT, the samples exhibited low thermal diffusivities ranging from 0.1 to 0.3 mm^2/s yielding thermal conductivity values consistently below 0.050 W.m^{-1}.K^{-1}. Higher temperature thermal diffusivities were further measured up to 500°C and the data (0.2–0.4 mm^2/s) was used to calculate thermal conductivities yielding between 0.050–0.107 W.m^{-1}.K^{-1}. The higher thermal conductivity of P10-A-1000 (Figure 9B) can be interpreted in terms of microstructural difference, for example, available large voids and cavities compared to the other samples, increasing the thermal conductivity by extending the photon mean free-path length.[47]

These values are comparable to similar ceramic aerogels systems reported in the literature such as alumina aerogel (0.298 W.m^{-1}.K^{-1} at 800°C),[48] silica aerogel (0.122 W.m^{-1}.K^{-1} at 400°C),[48] pure BN aerogel (~0.035 W.m^{-1}.K^{-1} at room temperature),[49] and BN/SiOC aerogel (0.2 W.m^{-1}.K^{-1} at 500°C).[42]

The experimental thermal camera setup is shown in Figure S6 and Figure 10A–D illustrates the backside

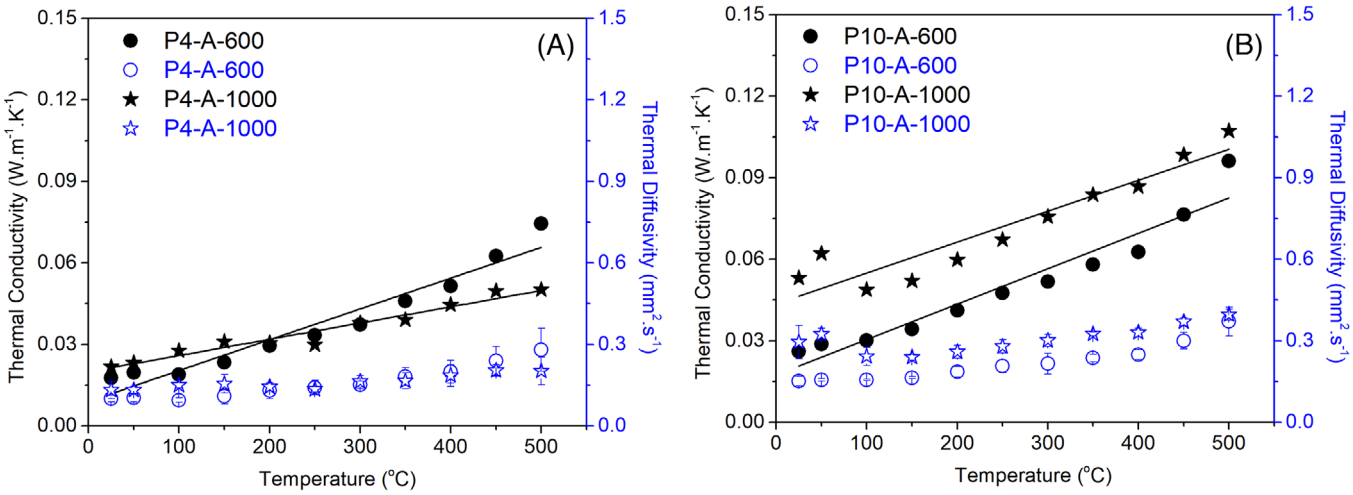

FIGURE 9 Temperature-dependent thermal conductivity and diffusivity values of the foam-aerogel composites from room temperature to 500°C (the measurable limit of the LFA device used). The bulk density of samples was taken as constant at all test temperatures (the solid line represents the linear fitting resulting in $R^2 = 0.87–0.95$).

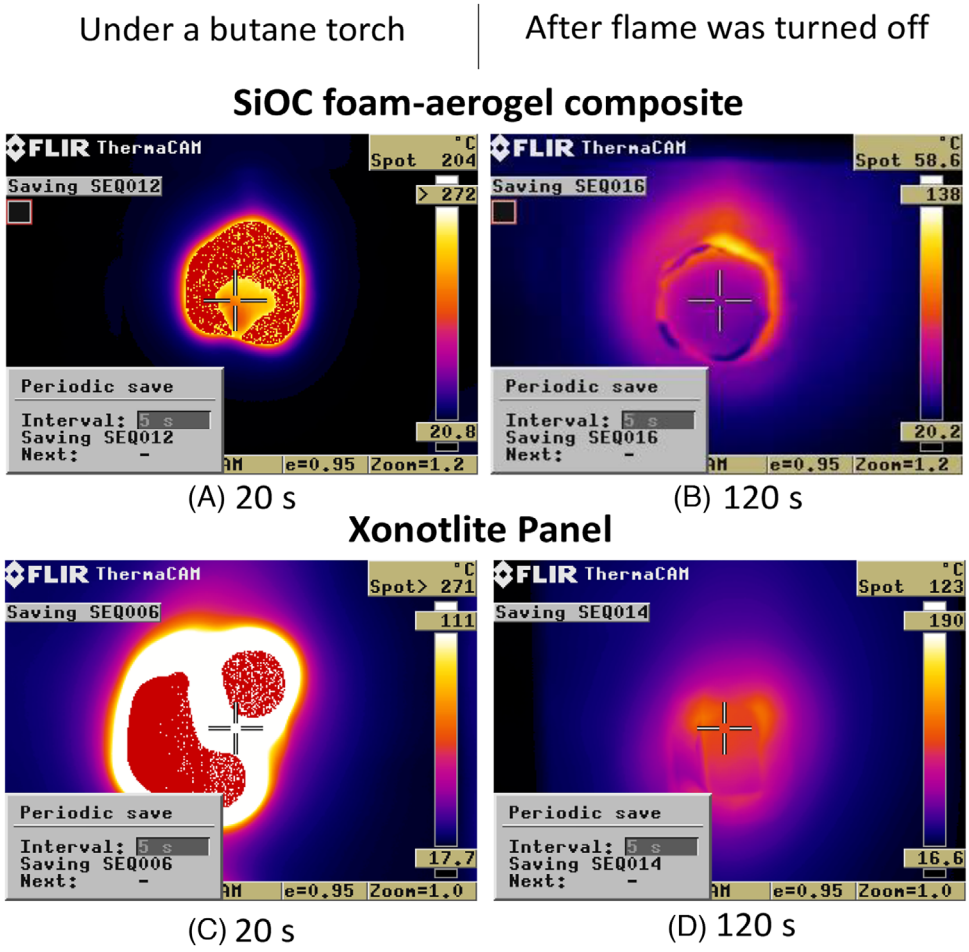

FIGURE 10 Temperature variation of backside for SiOC foam-aerogel composite and commercial Xonotlite panel; thermal infrared images of SiOC foam-aerogel composite (P4-A-1000) under a butane torch (A) at 20 s (spot temp.: 204°C) and (B) at 120 s after the flame was turned off (spot temp.: 58.6°C), thermal infrared images of commercial Xonotlite panel under a butane torch; (C) at 20 s (spot temp.: > 271°C), and (d) at 120 s after the flame was turned off (spot temp.: 123°C).

temperature of the tested samples. After being heated for 20 s, while the temperature of the butane torch was ~1200°C, from the backside of the SiOC foam-aerogel composite sample, only 204°C was recorded (Figure 10A), which was probably higher than 271°C (the highest temperature that can be read from the used infrared camera) for commercial xonotlite panel (see Figure 10B). After turning off the butane torch, at 120 s, while the backside temperature of the SiOC foam-aerogel rapidly dropped to 58.6°C (Figure 10C), the xonotlite panel remained hotter at 123°C (Figure 10D).

To assess the thermal stability, the butane-torch test was repeated three times, and the results are presented in Figure S7. Backside temperatures at 20 s were recorded as 147°C for 2nd cycle and 111°C for 3rd cycle. After turning off the flame, the backside temperatures were recorded as ~70°C at the end of 120 s. Remarkably, the monolith foam-aerogel composite remained intact and retained its original shape; only a color change due probably to oxidation, similar to other works,[50,51] was observable at the end of the 3rd cycle, see insets in Figure S8. Overall, the SiOC foam-aerogel composites demonstrated superb thermal insulation and excellent flame-retardant and insulation capacity even in ambient air (with a relative humidity of 82%), signifying a high potential for their high-temperature applications.

4 | CONCLUSIONS

This study focused on synthesizing commercial siloxane resin-derived foam-aerogel composites in polymeric, hybrid, and ceramic states. Specifically, polymer-derived foams were replicated from PU foams by impregnating & pyrolysis and effectively utilized as a structural framework for aerogels through CO_2 SC-Drying and, finally, pyrolysis at varying (600–1000°C) temperatures.

For the first time, the SiOC foam-aerogel composite pyrolyzed at 600°C showed complete impregnation of the foam cells by the solidified aerogel. Instead, foam-aerogel composite produced using parent foam pyrolyzed at 1000°C had cavities around struts. SiOC ceramic composite exhibited an SSA of 169 m^2/g, while it was 503 m^2/g for hybrid composite and 644 m^2/g for polymeric one. The foam-aerogel composites revealed adjustable surface characteristics, providing hydrophobic (polymeric and hybrid states) and hydrophilic (ceramic state) features.

While the SiOC foam-aerogel composites consistently demonstrated a very low relative density of ~0.2 g/cm^3, that is, a total porosity of approximately 90 vol%, the samples exhibited excellent specific compressive strength, reaching around 2 MPa. The study unveiled the potential application of these composites as thermal insulators, displaying low thermal conductivities of 0.02 $W \cdot m^{-1} \cdot K^{-1}$ at room temperature and 0.05 $W \cdot m^{-1} \cdot K^{-1}$ at 500°C. Besides, when subjected to direct exposure to a butane flame gun with a flame temperature of ~1200°C, the back side of a 5 mm-thick foam-aerogel composite recorded a temperature of only ~200°C. This temperature was lower than that observed in a comparable commercial insulator panel tested under identical conditions.

ACKNOWLEDGMENTS

This study was supported by the Scientific and Technological Research Council of Turkey (TUBITAK) under Grant number 122M533. The authors thank TUBITAK for their support. We recognize the Izmir Institute of Technology, and the Center for Materials Research for the N2 sorption data analyses, TGA, XRD, RAMAN, and SEM investigations. The authors thank Dr. Rajat Chaudhary from the University of Trento, Italy for the mechanical tests. Oyku Icin and Cekdar Vakif Ahmetoglu would like to acknowledge the financial support of AFOSR with the program manager, Dr. Ali Sayir, through grant # FA9550-21-1-0279.

CONFLICT OF INTEREST STATEMENT

The authors declare no conflict of interest.

ORCID

Oyku Icin https://orcid.org/0000-0002-8228-7409
Gian Domenico Soraru https://orcid.org/0000-0002-0453-3379
Cekdar Vakifahmetoglu https://orcid.org/0000-0003-1222-4362

REFERENCES

1. Karakuscu A, Ponzoni A, Comini E, Sberveglieri G, Vakifahmetoglu C. SiC foams decorated with SnO_2 nanostructures for room temperature gas sensing. Int J Appl Ceram Technol. 2014;11(5):851–57. https://doi.org/10.1111/ijac.12295
2. Vakifahmetoglu C, Semerci T, Gurlo A, Soraru GD. Polymer derived ceramic aerogels. Curr Opin Solid State Mater Sci. 2021;25(4):100936. https://doi.org/10.1016/j.cossms.2021.100936
3. Hasegawa G, Kanamori K, Nakanishi K. Porous polymer-derived ceramics: flexible morphological and compositional controls through sol–gel chemistry. J Am Ceram Soc. 2022;105(1):5–34. https://doi.org/10.1111/jace.18130
4. Manoj Kumar BV, Kim YW. Processing of polysiloxane-derived porous ceramics: a review. Sci Technol Adv Mater. 2010;11(4):44303. https://doi.org/10.1088/1468-6996/11/4/044303
5. Semerci T, Dizdar KC, Kulkarni A, Dispinar D, Soraru GD, Vakifahmetoglu C. Polymer-derived ceramic molten metal filters. J Mater Sci. 2022;57(31):14723–34. https://doi.org/10.1007/s10853-022-07542-9
6. Li C, Chen Z, Dong W, Lin L, Zhu X, Liu Q, et al. A review of silicon-based aerogel thermal insulation materials: performance optimization through composition and microstructure.

J Non-Cryst Solids. 2021;553:120517. https://doi.org/10.1016/j.jnoncrysol.2020.120517

7. Pradeep VS, Ayana DG, Graczyk-Zajac M, Soraru GD, Riedel R. High rate capability of SiOC ceramic aerogels with tailored porosity as anode materials for Li-ion batteries. Electrochim Acta. 2015;157:41–45. https://doi.org/10.1016/j.electacta.2015.01.088
8. Mazrouei-Sebdani Z, Begum H, Schoenwald S, Horoshenkov K V, Malfait WJ. A review on silica aerogel-based materials for acoustic applications. J Non-Cryst Solids. 2021;562:120770. https://doi.org/10.1016/j.jnoncrysol.2021.120770
9. Moreno-Castilla C, Maldonado-Hódar FJ. Carbon aerogels for catalysis applications: an overview. Carbon NY. 2005;43(3):455–65. https://doi.org/10.1016/j.carbon.2004.10.022
10. Maleki H. Recent advances in aerogels for environmental remediation applications: a review. Chem Eng J. 2016;300:98–118. https://doi.org/10.1016/j.cej.2016.04.098
11. Bheekhun N, Talib A, Rahim A, Hassan MR. Aerogels in aerospace: an overview. Adv Mater Sci Eng. 2013;2013. https://doi.org/10.1155/2013/406065
12. Du B, Hong C, Wang A, Zhou S, Qu Q, Zhou S, et al. Preparation and structural evolution of SiOC preceramic aerogel during high-temperature treatment. Ceram Int. 2018;44(1):563–70. https://doi.org/10.1016/j.ceramint.2017.09.212
13. Tong Z, Yan B, Zhang B, Xu H, Li X, Ji H. Preparation and textural evolution: from organosilane aerogel to SiOC aerogels. Ceram Int. 2022;48(4):5468–75. https://doi.org/10.1016/j.ceramint.2021.11.091
14. Liao Y, Wu H, Ding Y, Yin S, Wang M, Cao A. Engineering thermal and mechanical properties of flexible fiber-reinforced aerogel composites. J Sol-Gel Sci Technol. 2012;63(3):445–56. https://doi.org/10.1007/s10971-012-2806-7
15. Yang X, Sun Y, Shi D, Liu J. Experimental investigation on mechanical properties of a fiber-reinforced silica aerogel composite. Mater Sci Eng A. 2011;528(13):4830–36. https://doi.org/10.1016/j.msea.2011.03.013
16. Lee KY, Mahadik DB, Parale VG, Park HH. Composites of silica aerogels with organics: a review of synthesis and mechanical properties. J Korean Ceram Soc. 2020;57(1):1–23. https://doi.org/10.1007/s43207-019-00002-2
17. Dai YJ, Tang YQ, Fang WZ, Zhang H, Tao WQ. A theoretical model for the effective thermal conductivity of silica aerogel composites. Appl Therm Eng. 2018;128:1634–45. https://doi.org/10.1016/j.applthermaleng.2017.09.010
18. Zhang H, Fang WZ, Wang X, Li YM, Tao WQ. Thermal conductivity of fiber and opacifier loaded silica aerogel composite. Int J Heat Mass Transf. 2017;115:21–31. https://doi.org/10.1016/j.ijheatmasstransfer.2017.08.006
19. Merillas B, Lamy-Mendes A, Villafañe F, Durães L, Rodríguez-Pérez MÁ. Polyurethane foam scaffold for silica aerogels: effect of cell size on the mechanical properties and thermal insulation. Mater Today Chem. 2022;26:101257. https://doi.org/10.1016/j.mtchem.2022.101257
20. Su R, Wang X, Wang D, Li L, Liang G, Zheng Z, et al. Preparation of carbon foam-reinforced carbon aerogels and their copyrolysis mechanism. Microporous Mesoporous Mater. 2021;319:111059. https://doi.org/10.1016/j.micromeso.2021.111059
21. Song Z, Zhao Y, Yuan M, Huang L, Yuan M, Cui S. Thermal insulation and moisture resistance of high-performance silicon aerogel composite foam ceramic and foam glass. Adv Eng Mater. 2022;24(8):2101508. https://doi.org/10.1002/adem.202101508
22. Merillas B, Villafañe F, Rodríguez-Pérez MÁ. Improving the insulating capacity of polyurethane foams through polyurethane aerogel inclusion: from insulation to superinsulation. Nanomaterials. 2022;12(13):2232. https://doi.org/10.3390/nano12132232
23. Renjith PK, Sarathchandran C, Sivanandan Achary V, Chandramohanakumar N, Sekkar V. Micro-cellular polymer foam supported silica aerogel: Eco-friendly tool for petroleum oil spill cleanup. J Hazard Mater. 2021;415:125548. https://doi.org/10.1016/j.jhazmat.2021.125548
24. Jiang Q, Liao X, Yang J, Wang G, Chen J, Tian C, et al. A two-step process for the preparation of thermoplastic polyurethane/graphene aerogel composite foams with multistage networks for electromagnetic shielding. Compos Commun. 2020;21:100416. https://doi.org/10.1016/j.coco.2020.100416
25. Kim BS, Choi J, Park YS, Qian Y, Shim SE. Semi-rigid polyurethane foam and polymethylsilsesquioxane aerogel composite for thermal insulation and sound absorption. Macromol Res. 2022;30(4):245–53. https://doi.org/10.1007/s13233-022-0026-8
26. Xie H, Yang W, Yuen ACY, Xie C, Xie J, Lu H, et al. Study on flame retarded flexible polyurethane foam/alumina aerogel composites with improved fire safety. Chem Eng J. 2017;311:310–17. https://doi.org/10.1016/j.cej.2016.11.110
27. Ye X, Chen Z, Ai S, Hou B, Zhang J, Zhou Q, et al. Microstructure characterization and thermal performance of reticulated SiC skeleton reinforced silica aerogel composites. Compos Part B Eng. 2019;177:107409. https://doi.org/10.1016/j.compositesb.2019.107409
28. Merillas B, Lamy-Mendes A, Villafañe F, Durães L, Rodríguez-Pérez MÁ. Silica-based aerogel composites reinforced with reticulated polyurethane foams: Thermal and mechanical properties. Gels. 2022;8(7):392. https://doi.org/10.3390/gels8070392
29. Liu H, Li T, Shi Y, Zhao X. Thermal insulation composite prepared from carbon foam and silica aerogel under ambient pressure. J Mater Eng Perform. 2015;24(10):4054–59. https://doi.org/10.1007/s11665-015-1686-8
30. Schwan M, Rößler M, Milow B, Ratke L. From fragile to resilient insulation: synthesis and characterization of aramid-honeycomb reinforced silica aerogel composite materials. Gels. 2015;2(1):1. https://doi.org/10.3390/gels2010001
31. Liu Y, Chen Z, Zhang J, Ai S, Tang H. Ultralight and thermal insulation carbon foam/SiO_2 aerogel composites. J Porous Mater. 2019;26(5):1305–12. https://doi.org/10.1007/s10934-019-00732-y
32. Zambotti A, Ionescu E, Gargiulo N, Caputo D, Vakifahmetoglu C, Santhosh B, et al. Processing of polymer-derived, aerogel-filled, SiC foams for high-temperature insulation. J Am Ceram Soc. 2023;106(8):4891–901. https://doi.org/10.1111/jace.19118
33. Semerci T, de Mello Innocentini MD, Marsola GA, Lasso PRO, Soraru GD, Vakifahmetoglu C. Hot air permeable preceramic polymer derived reticulated ceramic foams. ACS Appl Polym Mater. 2020;2(9):4118–26. https://doi.org/10.1021/acsapm.0c00734
34. Icin O, Semerci T, Soraru GD, Vakifahmetoglu C. Design and performance comparison of polymer-derived ceramic ambigels and aerogels. ACS Omega. 2023;8:32955–62. https://doi.org/10.1021/acsomega.3c04607

35. Stabler C, Reitz A, Stein P, Albert B, Riedel R, Ionescu E. Thermal properties of SiOC glasses and glass ceramics at elevated temperatures. Materials (Basel). 2018;11(2):279. https://doi.org/10.3390/ma11020279
36. Krüner B, Odenwald C, Jäckel N, Tolosa A, Kickelbick G, Presser V. Silicon oxycarbide beads from continuously produced polysilsesquioxane as stable anode material for lithium-ion batteries. ACS Appl Energy Mater. 2018;1(6):2961–70. https://doi.org/10.1021/acsaem.8b00716
37. Guo W, Icin O, Vakifahmetoglu C, Kober D, Gurlo A, Bekheet MF. Magnesium ion battery anode from polymer-derived SiOC nanobeads. Adv Funct Mater. 2023;33(48):2304933. https://doi.org/10.1002/adfm.202304933
38. Vakifahmetoglu C, Balliana M, Colombo P. Ceramic foams and micro-beads from emulsions of a preceramic polymer. J Eur Ceram Soc. 2011;31(8):1481–90. https://doi.org/10.1016/j.jeurceramsoc.2011.02.012
39. Vakifahmetoglu C, Colombo P. A direct method for the fabrication of macro-porous SiOC ceramics from preceramic polymers. Adv Eng Mater. 2008;10(3):256–59. https://doi.org/10.1002/adem.200700330
40. Icin O, Vakifahmetoglu C. Dye removal by polymer derived ceramic nanobeads. Ceram Int. 2021;47(19):27050–57. https://doi.org/10.1016/j.ceramint.2021.06.118
41. Jana P, Zera E, Sorarù GD. Processing of preceramic polymer to low density silicon carbide foam. Mater Des. 2017;116:278–86. https://doi.org/10.1016/j.matdes.2016.12.010
42. Yang H, Li C, Yue X, Huo J, Ye F, Liu J, et al. New BN/SiOC aerogel composites fabricated by the sol-gel method with excellent thermal insulation performance at high temperature. Mater Des. 2020;185:108217. https://doi.org/10.1016/j.matdes.2019.108217
43. An Z, Zhang R, Fang D. Synthesis of monolithic SiC aerogels with high mechanical strength and low thermal conductivity. Ceram Int. 2019;45(9):11368–74. https://doi.org/10.1016/j.ceramint.2019.02.216
44. Hou X, Zhang R, Fang D. Novel whisker-reinforced Al_2O_3–SiO_2 aerogel composites with ultra-low thermal conductivity. Ceram Int. 2017;43(12):9547–51. https://doi.org/10.1016/j.ceramint.2017.04.043
45. Li Z, Cheng X, He S, Shi X, Gong L, Zhang H. Aramid fibers reinforced silica aerogel composites with low thermal conductivity and improved mechanical performance. Compos Part A Appl Sci Manuf. 2016;84:316–25. https://doi.org/10.1016/j.compositesa.2016.02.014
46. Zhao Y, Li Y, Zhang R. Silica aerogels having high flexibility and hydrophobicity prepared by sol-gel method. Ceram Int. 2018;44(17):21262–68. https://doi.org/10.1016/j.ceramint.2018.08.173
47. Wang E, Shi Z, Chen M, Tang S, Zhang X, Zhang W. Investigation of effective thermal conductivity of SiC foam ceramics with various pore densities. 2022;20(1):58–65. https://doi.org/10.1515/phys-2022-0003
48. Poco JF, Satcher JH, Hrubesh LW. Synthesis of high porosity, monolithic alumina aerogels. J Non-Cryst Solids. 2001;285(1):57–63. https://doi.org/10.1016/S0022-3093(01)00432-X
49. Li G, Zhu M, Gong W, Du R, Eychmüller A, Li T, et al. Boron nitride aerogels with super-flexibility ranging from liquid nitrogen temperature to 1000°C. Adv Funct Mater. 2019;29(20):1900188. https://doi.org/10.1002/adfm.201900188
50. Wang H, Chen Z, Su D. Lightweight and large-scale rGO reinforced SiBCN aerogels with hierarchical cellular structures exposed to high-temperature environments. J Mater Sci Technol. 2024;179:145–54. https://doi.org/10.1016/j.jmst.2023.09.014
51. Sun X, Zhu W, Wang H, Yan X, Su D. In situ formation of the TiCN phase in SiBCN ceramic aerogels enabling superior thermal and structural stability up to 1800°C. ACS Appl Mater Interfaces. 2023;15(9):12221–31. https://doi.org/10.1021/acsami.2c22601

SUPPORTING INFORMATION

Additional supporting information can be found online in the Supporting Information section at the end of this article.

How to cite this article: Icin O, Abebe AM, Soraru GD, Vakifahmetoglu C. SiOC foam-aerogel composites: Optimal balance of lightness and excellent thermal insulation. J Am Ceram Soc. 2024;107:6729–40. https://doi.org/10.1111/jace.19967